J. Phys. D: Appl. Phys. **45** (2012) 465205 (9pp) doi:10.1088/0022-3727/45/46/465205

The effect of the driving frequencies on the electrical asymmetry of dual-frequency capacitively coupled plasmas

Ihor Korolov[1], Zoltán Donkó[1], Uwe Czarnetzki[2] and Julian Schulze[2]

[1] Institute for Solid State Physics and Optics, Wigner Research Centre for Physics, Hungarian Academy of Sciences, 1121 Budapest, Konkoly Thege Miklós str. 29-33, Hungary
[2] Institute for Plasma and Atomic Physics, Ruhr University Bochum, 44780 Bochum, Germany

E-mail: korolov.ihor@wigner.mta.hu

Received 24 July 2012, in final form 12 September 2012
Published 26 October 2012
Online at stacks.iop.org/JPhysD/45/465205

Abstract
In capacitively coupled radio frequency discharges driven by two consecutive phase-locked harmonics, the electrical asymmetry effect (EAE) allows one to generate a dc self-bias as a function of the phase shift, θ, between the driving harmonics. If the two frequencies are chosen to be 13.56 and 27.12 MHz, the mean ion energy at both electrodes can be varied by a factor of about 2 by tuning θ at nearly constant ion flux. Until now the EAE has only been investigated in discharges operated at a fundamental frequency of $f = 13.56$ MHz. Here, we study the effect of changing this fundamental frequency on the performance of the EAE, i.e. on the electrical generation of a dc self-bias, the control range of the mean ion energy, and on the ion flux at both electrodes as a function of θ, by kinetic particle-in-cell/Monte Carlo simulations and theoretical modelling. We use argon gas and cover a wide range of fundamental frequencies (0.5 MHz $\leqslant f \leqslant$ 60 MHz) and secondary electron yields. We find that the performance of the EAE is significantly worse at lower frequencies, i.e. the control range of the dc self-bias and, thus, the control range of the mean ion energy are strongly reduced. Based on the analytical model (i) the enhanced charged dynamics at lower frequencies and (ii) the transition of the electron heating mode induced by changing f are found to be the reasons for this effect.

(Some figures may appear in colour only in the online journal)

1. Introduction

Capacitively coupled radio frequency (CCRF) discharges play a basic role in modern plasma processing technologies [1, 2]. The control of ion properties, namely, the ion flux, Γ_i, and the mean ion energy, $\langle E_i \rangle$, is particularly important for such applications. This separate control has motivated studies of discharges driven by two, or even multiple frequencies [3–9], and the development of hybrid (inductive + capacitive) sources including customized bias voltage waveforms [10–14, 15–18]. At high driving frequencies and large substrate surface areas, electromagnetic standing wave effects can cause radial inhomogeneities of the ion flux across the electrodes [19]. These effects can be prevented by dielectric lenses [20] or graded conductivity electrodes [21], but generally cause problems at high driving frequencies.

A widely used concept to realize this separate control is driving one electrode by a waveform, $\phi(t)$, which is the superposition of two radio frequency voltages:

$$\phi(t) = \phi_{\mathrm{lf}} \cos(2\pi f_{\mathrm{lf}} t) + \phi_{\mathrm{hf}} \cos(2\pi f_{\mathrm{hf}} t). \qquad (1)$$

Here ϕ_{lf} and ϕ_{hf} is, respectively, the amplitude of the low-frequency (f_{lf}) and the high-frequency (f_{hf}) voltage waveform. In 'classical' dual-frequency (df) discharges, two significantly

different frequencies, such as 1 and 100 MHz, are chosen with $\phi_{\rm lf} > \phi_{\rm hf}$. This approach is based on the idea that the high-frequency voltage amplitude determines the electron heating and, thus, the ion flux, whereas the low-frequency (lf) amplitude determines the ion energy at the electrodes. This concept was demonstrated to perform well only within narrow parameter ranges and to generally fail due to the frequency coupling [22–26] and the effect of secondary electrons [27, 28].

An almost ideal separate control of these ion properties can be realized via the electrical asymmetry effect (EAE) [29]. The EAE allows one to generate a dc self-bias, η, as a function of the phase shift, θ, between two phase-locked consecutive driving harmonics even in geometrically symmetric discharges. In practice, one electrode is driven by the following voltage waveform:

$$\phi(t) = \phi_{\rm lf}\cos(2\pi f t + \theta) + \phi_{\rm hf}\cos(4\pi f t). \qquad (2)$$

We note that, a complex matching circuit is required to drive one electrode with such a voltage waveform [30]. Generally, the voltage waveform at the electrode does not correspond to the generator output. These differences will be affected by the choice of the driving frequencies. Such problems can be solved by automated feedback systems that measure the voltage at the electrode and adjust the generator output to realize a certain waveform at the electrode [12].

For a fundamental frequency of $f = 13.56$ MHz, it was found that the mean ion energy can be changed by a factor of about 2 at constant ion flux by tuning θ from 0° to 90° [29–31]. In this way, the frequency coupling and parasitic effects of secondary electrons are widely avoided [28]. The strongest self-bias is generated electrically at (or near) $\theta = 0°$ (negative bias) and $\theta = 90°$ (positive bias). Reaching a high self-bias is advantageous, since it allows one to realize a wider range of ion energy control. Thus, most of the optimization studies of the EAE have targeted increasing the value of the self-bias. The EAE has been investigated in different gases, in Ar [30, 32, 33], in hydrogen [34], in oxygen [35] and in CF_4 [36]. Optimization of the ratio of the voltage amplitudes ($\phi_{\rm hf}/\phi_{\rm lf}$) was reported in [37], while the possibilities of using more than two driving frequencies have been explored in [38]. The effect of secondary electrons has been studied in [28], in comparison with classical df discharges.

Until now all investigations of electrically asymmetric df plasmas have been limited to the fundamental frequency of $f = 13.56$ MHz. However, for applications also other frequencies are often used [1, 2, 39–43]. Thus, in this work we investigate the effect of changing the fundamental driving frequency on the performance of the EAE, i.e. on the electrical generation of the dc self-bias, the control range of the mean ion energy, and the ion flux at both electrodes as a function of θ, by kinetic particle-in-cell/Monte Carlo simulations and theoretical modelling.

Our studies cover the frequency range 0.5 MHz $\leqslant f \leqslant$ 60 MHz and a wide domain of ion induced secondary electron yields. The paper is structured as follows. Section 2 describes the simulation method as well as the model and specifies the range of parameters covered in the frame of this work. The results are presented in section 3, while section 4 briefly summarizes our conclusions.

2. Simulation method and discharge model

2.1. Simulation method

Our simulations are based on a one-dimensional (1D3V) bounded plasma particle-in-cell (PIC) code complemented by a Monte Carlo treatment of collision processes (often referred to as 'PIC/MCC' approach) [44–46]. Our studies are carried out using argon gas. The cross sections for electron–neutral and ion–neutral collision processes are taken from [47].

The discharge is driven by the voltage waveform defined by equation (2). The low- and high-frequency amplitudes are chosen to be identical, i.e. $\phi_{\rm lf} = \phi_{\rm hf} = \phi_0$. The dc self-bias is determined in an iterative manner to ensure that the (positive and negative) charged particle fluxes to either of the two electrodes, averaged over one lf period, are equal. The simulations are performed for an electrode gap of $d = 2.5$ cm at a neutral gas pressure of $p = 50$ Pa.

At the planar, parallel and infinite electrodes, electrons are reflected with a probability of 20% [48], and we account for the ion-induced emission of secondary electrons using γ of 0, 0.1 and 0.4. In this way, we study the effect of using different electrode materials and generally the effect of γ-electrons on the performance of the EAE. While $\gamma = 0.1$ corresponds to typical metal surfaces, $\gamma = 0.4$ corresponds to dielectric or semiconductor electrodes. In our code, fast electrons are moved with a smaller time step compared with slow electrons, to ensure that the Courant condition is fulfilled for all electrons, while maintaining an acceptable runtime of the code.

A pressure of 50 Pa is chosen to maximize the frequency interval, where the simulations converge at otherwise constant parameters. In this way we ensure to study only the effect of the fundamental frequency on the EAE. At lower pressures, the simulations do not converge at low frequencies and at higher pressures the simulations diverge at high frequencies. Certainly, similar investigations at lower pressures relevant for etching [2] and at higher pressures relevant for plasma enhanced chemical vapour deposition [49] would be interesting, but are outside the scope of this work. However, the conclusions drawn here regarding the effect of the frequency on the EAE are believed to be rather general, although one has to note that using electronegative discharges—as in a number of plasma processing applications—additional physical effects, e.g. electron heating in the bulk electric field [50], may modify the results.

2.2. Analytical model

The interpretation of the simulation results is performed on the basis of an analytical model of CCRF discharges, which is described in detail elsewhere [51]. Here, only its result for the dc self-bias, η, is used:

$$\eta = -\frac{\phi_{\rm max} + \varepsilon\phi_{\rm min}}{1+\varepsilon} + \frac{\phi_{\rm sp}^{\rm f} + \varepsilon\phi_{\rm sg}^{\rm f}}{1+\varepsilon} + \frac{\phi_{\rm max}^{\rm b} + \varepsilon\phi_{\rm min}^{\rm b}}{1+\varepsilon} \approx -\frac{\phi_{\rm max} + \varepsilon\phi_{\rm min}}{1+\varepsilon}. \qquad (3)$$

Here, $\phi_{\rm max}$ and $\phi_{\rm min}$ are the maximum and the minimum of the driving voltage waveform, $\phi(t)$, respectively, while

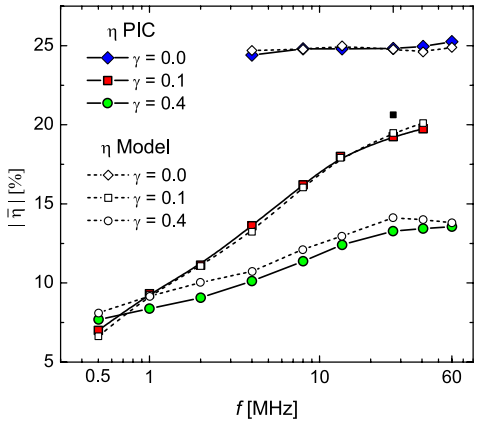

Figure 1. Absolute value of the normalized dc self-bias, $\bar{\eta}$, as a function of the fundamental driving frequency, f, for $\phi_0 = 200$ V and $\gamma = 0, 0.1$ as well as $\phi_0 = 80$ V, $\gamma = 0.4$ resulting from the PIC simulation (solid lines) and from the analytical model using equation (3) (dashed lines). The black square corresponds to the parameter combination $\phi_0 = 80$ V and $\gamma = 0.1$. $\theta = 0^\circ$ and $p = 50$ Pa are chosen in all cases. Note that the self-bias is negative at $\theta = 0^\circ$.

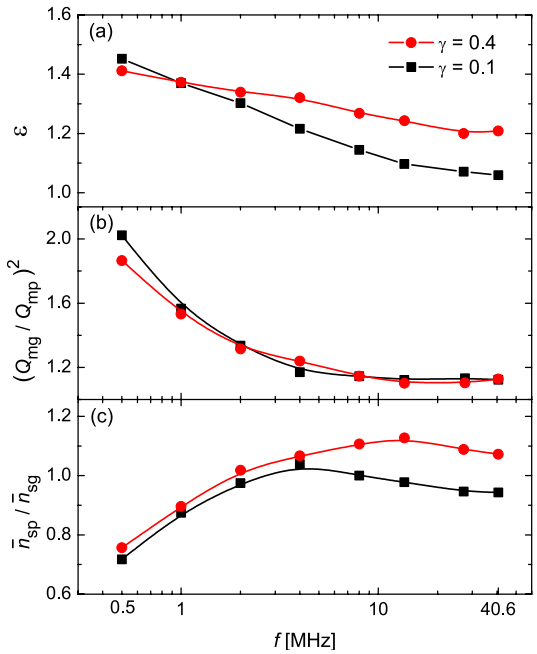

Figure 2. (*a*) Symmetry parameter as a function of the fundamental driving frequency, f, for $\phi_0 = 200$ V, $\gamma = 0.1$ and $\phi_0 = 80$ V, $\gamma = 0.4$. Corresponding values of (*b*) the square of the ratio of the maximum charges in the sheath at the grounded and powered electrode, $(Q_{mg}/Q_{mp})^2$, and (*c*) the ratio of the spatially averaged ion densities in the sheaths, $\overline{n}_{sp}/\overline{n}_{sg}$.

ϕ^{f}_{sp} and ϕ^{f}_{sg} are the floating potentials at the powered and grounded electrode. ϕ^{b}_{max} and ϕ^{b}_{min} are the voltage drops across the plasma bulk at the time of maximum and minimum applied voltages, respectively. In electropositive low pressure discharges such as investigated here, the first term dominates and the other terms can be neglected. ε is the symmetry parameter defined as the ratio of the maximum sheath voltages at both electrodes, $\hat{\phi}_{sp}$ and $\hat{\phi}_{sg}$. For equal electrode surface areas it is given by

$$\varepsilon = \left|\frac{\hat{\phi}_{sg}}{\hat{\phi}_{sp}}\right| \approx \frac{\overline{n}_{sp}}{\overline{n}_{sg}}\left(\frac{Q_{mg}}{Q_{mp}}\right)^2. \qquad (4)$$

Here, $\overline{n}_{sg}$ and $\overline{n}_{sp}$ are the spatially averaged ion density in the sheath at the grounded and powered electrodes, while Q_{mg} and Q_{mp} are the maximum (uncompensated) charge in the respective sheath.

In the following, input parameters in terms of the floating potentials, bulk voltages, and the symmetry parameter are taken from the simulations to calculate the self-bias via equation (3). Moreover, the self-bias normalized by $2\phi_0$, i.e. $\bar{\eta} = \eta/(2\phi_0)$, is discussed.

3. Results

Figure 1 shows the absolute value of the normalized dc self-bias, $|\bar{\eta}|$, as a function of the fundamental driving frequency, f, at $\theta = 0^\circ$ and $p = 50$ Pa, for secondary yields of $\gamma = 0$, 0.1 and 0.4. The solid lines and symbols show the simulation results, whereas the dashed lines and open symbols correspond to the model calculations using equation (3). At or close to $\theta = 0^\circ$ the strongest bias is generated for a given frequency [52]. The rf voltage is kept constant at $\phi_0 = 200$ V for $\gamma = 0$, 0.1 and at $\phi_0 = 80$ V for $\gamma = 0.4$. The frequency range covers the interval from $f = 0.5$ to 60 MHz. When f is changed, the second driving frequency is changed accordingly to ensure that always two consecutive harmonics are used. At fixed voltage amplitude, the frequency range is limited by a very slow convergence of the simulations at low frequencies and a divergence at high frequencies. This is similar to experiments, where no discharge can be ignited at 50 Pa for certain voltage amplitudes at low frequencies and arcing occurs at high frequencies. The voltage amplitudes are chosen to (i) be constant for a given γ to study only the effect of changing the frequency on the EAE and to (ii) maximize the frequency range, where the simulations converge. This requires different voltages for different γ-coefficients, again similar to experimental findings.

Similar to previous investigations using $f = 13.56$ MHz [29–31] a self-bias of 25% of the total driving voltage amplitude is found for $\gamma = 0$. Within the frequency range of convergence this value is essentially constant and will not be discussed further. Convergence is not found at frequencies below 4 MHz, since sheath heating becomes inefficient and no secondary electrons are included to sustain the discharge in γ-mode. Completely neglecting secondary electron emission, however, is unrealistic so that only the results for the two values of $\gamma = 0.1$ and 0.4 will be discussed in detail in the following.

Figure 2 shows the symmetry parameter, ε, as well as the following terms in equation (4) required to calculate ε as a function of f for $\gamma = 0.1$ and 0.4: the squared ratio of the maximum charges, $(Q_{mg}/Q_{mp})^2$, and the mean ion densities, $\overline{n}_{sp}/\overline{n}_{sg}$, in both sheaths, obtained from the simulations. The frequency range 0.5 MHz $\leqslant f \leqslant$ 40.6 MHz is shown.

First we discuss the effect of γ at high frequencies: at $f \geqslant 27.12$ MHz and $\theta \approx 0^\circ$ the strongest (negative) self-bias is generated via the EAE for a given value of γ. However, its

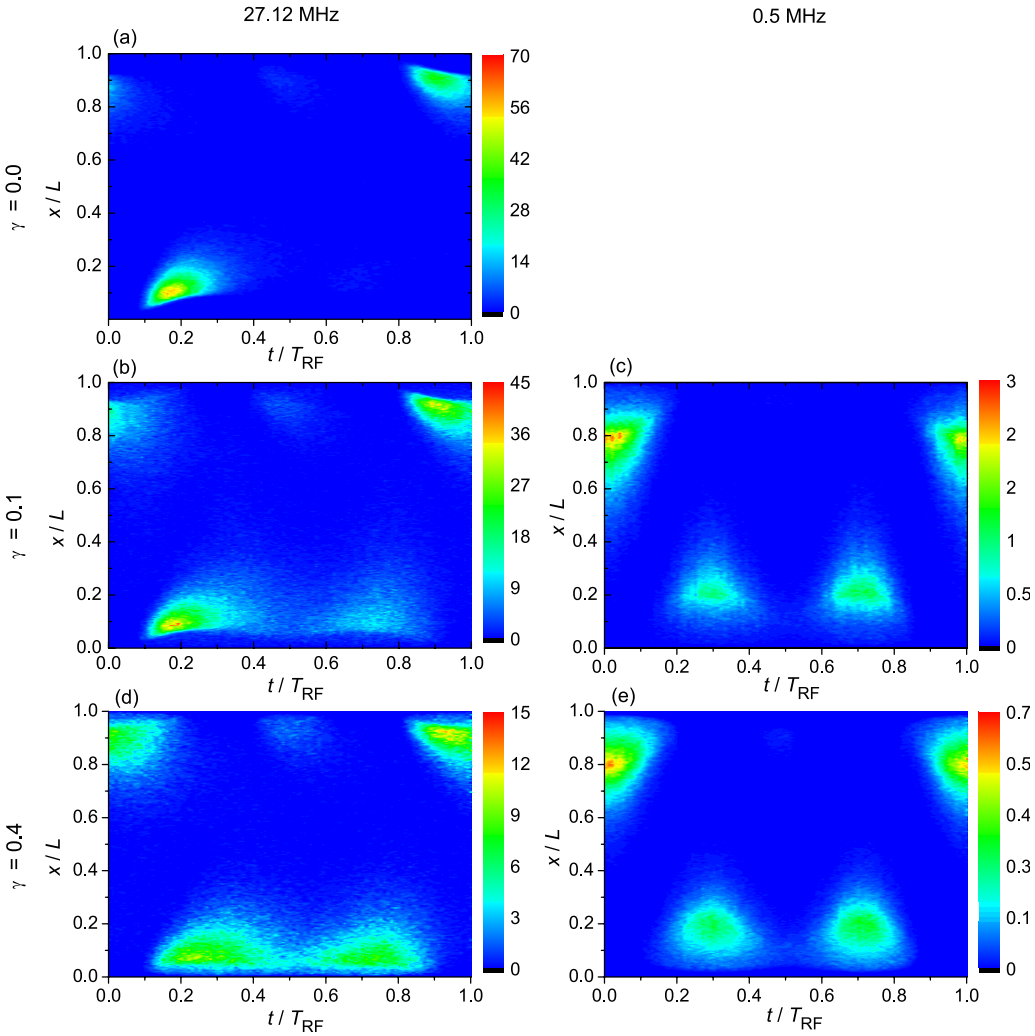

Figure 3. Spatio-temporal distribution of the ionization rate obtained from the simulations in the discharges operated at (*a*) $f = 27.12\,\mathrm{MHz}$, $\gamma = 0$; (*b*) $f = 27.12\,\mathrm{MHz}$, $\gamma = 0.1$, (*c*) $f = 0.5\,\mathrm{MHz}$, $\gamma = 0.1$, (*d*) $f = 27.12\,\mathrm{MHz}$, $\gamma = 0.4$ and (*e*) $f = 0.5\,\mathrm{MHz}$, $\gamma = 0.4$. The powered electrode is located at the bottom of the graphs, $x = 0$, while the position $x/L = 1$ corresponds to the grounded electrode. The ionization rate is given in units of $10^{21}\,\mathrm{m^{-3}\,s^{-1}}$.

magnitude is strongly affected by the choice of γ. It is reduced from $|\bar{\eta}| \approx 25\%$ at $\gamma = 0$ to $|\bar{\eta}| \approx 19\%$ at $\gamma = 0.1$ and finally to $|\bar{\eta}| \approx 13\%$ at $\gamma = 0.4$. In order to prove that this decrease is caused by the change of γ and not by the different voltage amplitudes we have also carried out an additional simulation with $\phi_0 = 80\,\mathrm{V}$ and $\gamma = 0.1$, at $f = 27.12\,\mathrm{MHz}$. This is confirmed: the solid black data point shown in figure 1 corresponding to these latter parameter values is in the vicinity of that obtained at $\phi_0 = 200\,\mathrm{V}$ and $\gamma = 0.1$.

The decrease in the self-bias as a function of γ at a fixed frequency and phase shift is caused by the effect of γ on the spatio-temporal ionization dynamics, which is shown in figures 3(*a*), (*b*) and (*d*) for $f = 27.12\,\mathrm{MHz}$. For $\gamma = 0$, the discharge is operated in α-mode and ionization caused by the expanding sheaths dominates [53]. As $\eta < 0\,\mathrm{V}$, the time-averaged sheath voltage at the powered electrode (situated at $x = 0$) is higher compared with that at the grounded electrode. Thus, for $\gamma > 0$ the acceleration and multiplication of secondary electrons in the sheath is more effective at the powered electrode. Consequently, more ionization by γ-electrons at the times of high sheath voltage within the rf period is found at the powered electrode. Additionally, ionization by the expanding sheath is observed. At the lower value of $\gamma = 0.1$ the latter ionization mechanism dominates, i.e. the discharge is operated mainly in the α-mode. By increasing γ a transition into the γ-mode is induced [53], so that ionization by secondary electrons dominates at $\gamma = 0.4$. In the γ-mode and for $\eta < 0\,\mathrm{V}$, significantly more ionization is observed at the powered compared with the grounded electrode. This asymmetry of the spatio-temporal distribution of the ionization is stronger at $\gamma = 0.4$ compared with 0.1. Consequently, for $\gamma = 0.4$ the mean ion density in the sheath adjacent to the powered electrode is higher compared with that at the grounded electrode. This affects the discharge symmetry, i.e. ε increases due to an increase in $\overline{n}_{\mathrm{sp}}/\overline{n}_{\mathrm{sg}}$ (see figure 2). According to equation (3) this will cause the self-bias to decrease, if γ is increased. The increase in the symmetry parameter to $\varepsilon \approx 1.2$ at high frequencies corresponds to a higher maximum sheath voltage at the grounded electrode compared with that at the powered electrode. This enhances

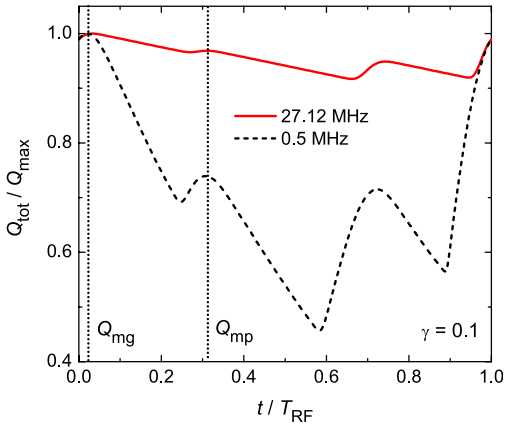

Figure 4. The total net charge in the discharge at $f = 0.5$ MHz and 27.12 MHz, within one rf period ($T_{RF} = 1/f$), normalized by its maximum value. $\gamma = 0.1$ for both cases. The vertical dashed lines show the position of the maximum charge in the sheaths at the powered (Q_{mp}) and grounded (Q_{mg}) electrodes.

the ionization by secondary electrons at the grounded electrode at the time of maximum sheath voltage relative to the time of maximum sheath voltage at the powered electrode and partly compensates the increase in $\overline{n}_{sp}/\overline{n}_{sg}$. However, at high frequencies the symmetry parameter is close to unity for both values of γ, so that the effect of the different time-averaged sheath voltages on the ionization dynamics is stronger compared with the effect of the different maximum sheath voltages.

Next we explore the effect of the driving frequencies: for both values of $\gamma > 0$, a strong decrease in the self-bias is induced by lowering the fundamental driving frequency. At $\gamma = 0.1$, $|\bar{\eta}|$ is reduced from 19% to 7%. This decrease is caused by the more pronounced charge dynamics [52] within the lf period at low compared with high driving frequencies. Figure 4 shows the total uncompensated positive charge in the plasma, Q_{tot}, normalized by its maximum, Q_{max}, as a function of time within one lf period. Time is normalized by the duration of one lf period, T_{RF}, for 27.12 MHz and 0.5 MHz. Note that T_{RF} is strongly different at 0.5 and 27.12 MHz. Most of the time the uncompensated charge decreases linearly as a function of time, since ions are continuously lost to the electrodes at the Bohm flux. However, when one sheath collapses, electrons are lost to one electrode and the charge increases again. At $\theta = 0^\circ$ two sheath collapses occur at the grounded electrode and one collapse occurs at the powered electrode within one lf period. Thus, the total net charge exhibits three maxima as a function of time, within one lf period. For both frequencies, the absolute maximum of the charge is found, when the sheath at the powered electrode collapses and the sheath at the grounded electrode is fully expanded. This charge corresponds to Q_{mg}. Q_{mp} is found at times of sheath collapse at the grounded electrode. The modulation of the total net charge as a function of time is significantly stronger at the lower frequency. At $f = 0.5$ MHz this modulation is about 50%. This is a notably high value, especially considering that some discharge models assume that the total net charge is (nearly) constant. At the higher frequency case, $f = 27.12$ MHz, the modulation of the net charge with time remains below 10%.

The stronger charge dynamics at lower frequencies is caused by the longer time between two consecutive sheath collapses, i.e. the longer duration of one lf period. More ions are lost between two collapses and the total charge decreases to lower values compared with the high-frequency scenario. Consequently, the ratio of the maximum charges, Q_{mg}/Q_{mp}, increases at lower frequencies such as shown in figure 2. This affects the symmetry of the discharge. According to equation (4) the symmetry parameter increases at lower fundamental frequencies due to the more pronounced charge dynamics (figure 4), i.e. the maximum sheath voltage at the grounded electrode becomes higher compared with that at the powered electrode. This, in turn, affects the ionization dynamics at low frequencies shown in figures 3(*c*) and (*e*). At $f = 0.5$ MHz, sheath expansion heating of electrons becomes inefficient and the discharge is operated in γ-mode for both values of γ investigated, i.e. by decreasing the frequency a transition from an rf towards a dc discharge is observed. As the maximum sheath voltage at the grounded electrode is now significantly higher compared with that of the powered electrode ($\varepsilon \approx 1.45$ for $\gamma = 0.1$ and $\varepsilon \approx 1.4$ for $\gamma = 0.4$), more ionization by secondary electrons is observed at the grounded electrode, although the mean sheath voltage is higher at the powered electrode ($\eta < 0$ V). This causes $\overline{n}_{sp}/\overline{n}_{sg}$ to become less than unity (see figures 2 and 5), which affects the symmetry parameter in a way that partly compensates the effect of the charge dynamics. This is completely different compared with the high-frequency scenario at 27.12 MHz, where $\overline{n}_{sp}/\overline{n}_{sg} > 1$ for high values of γ (figures 2 and 5), since the effect of the time-averaged sheath voltages on the ionization dynamics dominates compared with the effect of the maximum sheath voltages, since ε is close to unity at high frequencies. This difference is illustrated in figure 5, that shows the time-averaged ion density profiles at 0.5 and 27.12 MHz for $\gamma = 0.4$ together with the maximum sheath widths and the values of $\overline{n}_{sp}/\overline{n}_{sg}$ in both cases.

The self-bias is significantly different for different values of γ at high frequencies, but becomes similar at low frequencies for both values of $\gamma > 0$ (figure 1). At high frequencies, the charge dynamics is weak independently of γ, i.e. $Q_{mg}/Q_{mp} \approx 1$, and changing γ affects $\overline{n}_{sp}/\overline{n}_{sg}$ and, thus, ε and η via its effect on the ionization dynamics. At low frequencies, the charge dynamics leads to $Q_{mg}/Q_{mp} > 1$ and causes $\overline{n}_{sp}/\overline{n}_{sg} < 1$ via its effect on the ionization dynamics caused by the different maximum sheath voltages. However, at low frequencies the ion flux is lower at $\gamma = 0.4$ compared with 0.1 due to the lower driving voltage of 80 V compared with 200 V. Thus, the charge dynamics is less pronounced at $\gamma = 0.4$ and the maximum sheath voltages are more similar. This causes $\overline{n}_{sp}/\overline{n}_{sg}$ to be similar in both cases, although more secondary electrons are emitted at the electrodes at $\gamma = 0.4$. Finally, this results in a similar self-bias at low frequencies for both values of γ.

Decreasing the fundamental driving frequency affects the central ion density, n_i, as shown in figure 6. A quadratic increase in n_i as a function of f is found, such as predicted by a global power balance in CCRF discharges [2]. The effect of changing f on the mean ion energy and flux at both electrodes

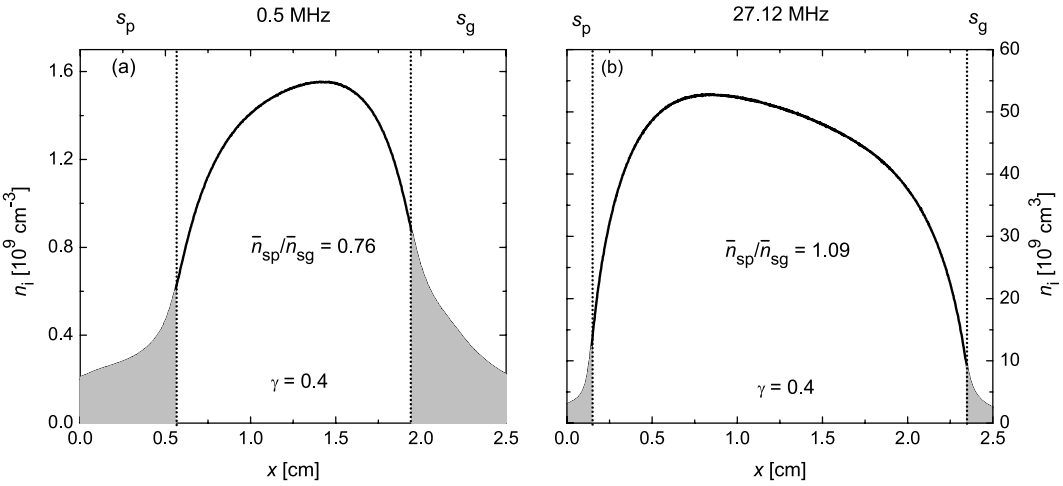

Figure 5. Distribution of the ion density obtained from the simulations in argon at 50 Pa, $\gamma = 0.4$: (a) 0.5 MHz and (b) 27.12 MHz. The powered electrode is situated at $x = 0$. The vertical dashed lines show the position of the sheath edges at maximum sheath expansion at the powered s_p and grounded s_g electrodes.

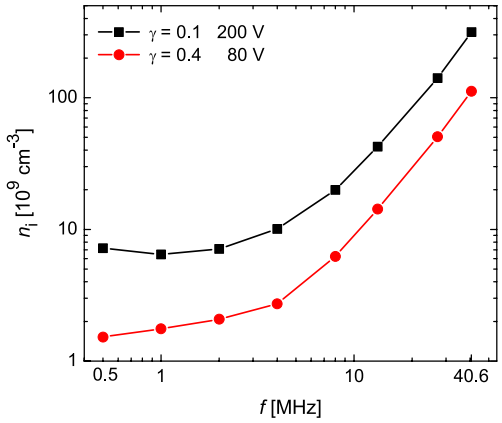

Figure 6. Central ion density, n_i, as a function of the fundamental driving frequency, f, resulting from the simulations at $\theta = 0^\circ$, for different values of γ.

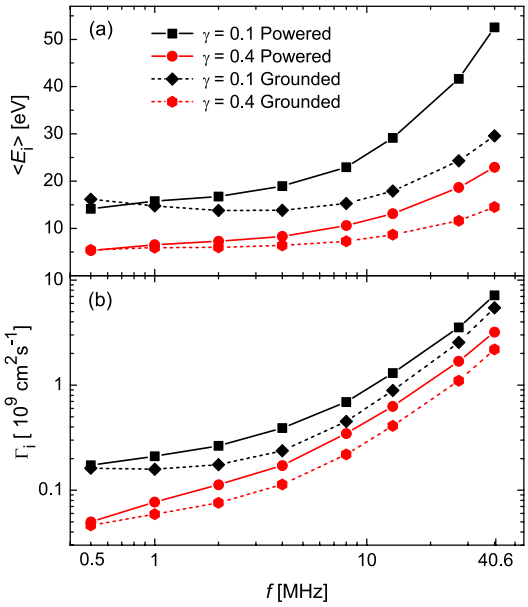

Figure 7. The mean ion energy, $\langle E_i \rangle$, (a), and ion flux, Γ_i, (b), at both electrodes as a function of the fundamental driving frequency, f, resulting from the simulations at $\theta = 0^\circ$, for different values of γ.

is plotted in figure 7. At both electrodes, the ion flux follows the quadratic behaviour of the central plasma density. It is generally higher at $\gamma = 0.1$ compared with $\gamma = 0.4$, due to the higher driving voltage of 200 V compared with 80 V. At high driving frequencies, the ion flux is higher at the powered compared with the grounded electrode for a given γ due to the asymmetric ionization dynamics caused by $\eta < 0$ V.

$\langle E_i \rangle$ decreases towards lower frequencies. This is caused by an increase in the sheath widths at lower frequencies, which is the consequence of a decrease of the ion density at fixed voltages. This causes the sheaths to become more collisional at lower frequencies and reduces the mean ion energy. For a given γ, $\langle E_i \rangle$ is significantly different at both electrodes at high frequencies, while it is almost identical at low frequencies. This is caused by the strong decrease in $|\bar{\eta}|$ towards lower frequencies.

The dependence of the self-bias voltage on the phase angle, which is the control parameter for the mean ion energy, is shown in figure 8 for different fundamental frequencies and $\gamma = 0.1$. The control range of the bias voltage is significantly reduced at lower frequencies due to the enhanced charge dynamics. Moreover, the functional dependence of η on θ is different at low and high driving frequencies. While the self-bias increases monotonically between 0° and 90° at high frequencies, it decreases slightly at small phase shifts and then increases at the lower values of f investigated. This is caused by the effect of θ on the charge and ionization dynamics. Figure 9 aids the understanding of this observation for $\gamma = 0.1$ at 1 and 27.12 MHz. At $\theta = 0^\circ$ the sheath adjacent to the grounded electrode collapses twice per lf period, while the sheath at the powered electrode collapses only once. The minimum sheath voltage during the second collapse at the grounded electrode increases as a function of θ due to a change in the driving voltage waveform until no electrons are lost to the grounded electrode during the second collapse at values of $\theta \approx 20^\circ$. This small angle effect (SAE) causes

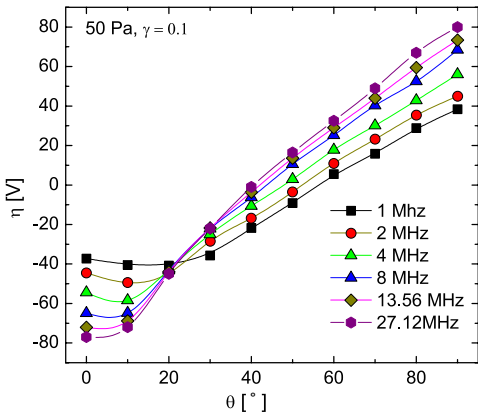

Figure 8. Simulation results for the self-bias as a function of the phase angle, θ, in a geometrically symmetric df discharge operated at different frequencies in a range 1–27.12 MHz, at 50 Pa, $\gamma = 0.1$.

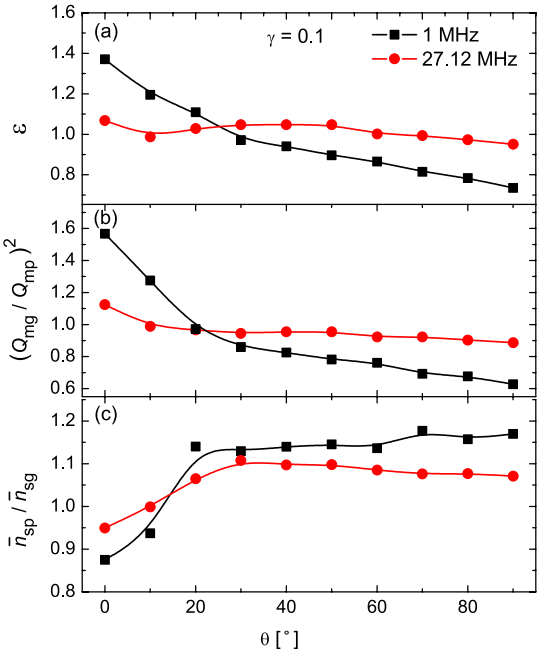

Figure 9. ε, $(Q_{mg}/Q_{mp})^2$, and $\bar{n}_{sp}/\bar{n}_{sg}$ as a function of θ for $f = 1$ MHz and 27.12 MHz, at $\gamma = 0.1$ and 50 Pa.

$(Q_{mg}/Q_{mp})^2 > 1$ for $\theta \leqslant 20^\circ$. As the charge dynamics is more pronounced at low frequencies, the SAE is more important at 1 MHz compared with 27.12 MHz, where $\varepsilon \approx 1$ independently of θ. An analogous effect happens for phase shifts around 90° with the role of both electrodes being reversed. The charge dynamics, i.e. $(Q_{mg}/Q_{mp})^2 \neq 1$, and, thus, the SAE affects the ionization dynamics in the way described before. Thus, $\bar{n}_{sp}/\bar{n}_{sg}$ also changes as a function of θ and partly compensates the effect of the charge dynamics on the discharge symmetry.

The reduced control range of the self-bias as a function of θ at low driving frequencies caused by the charge dynamics has important consequences for applications, since it causes a strong reduction of the control range of the mean ion energy at lower frequencies. Figure 10 shows that the mean ion energy changes by a factor of about 1.75 (between about 24 eV and 42 eV) as a function of θ at $f = 27.12$ MHz, while it changes only by a factor of about 1.2 at 1 MHz. Although the relative variations of the ion flux are reasonably small for all frequencies studied, this result implies that the EAE cannot be used effectively to control the mean ion energy in df CCRF discharges operated at low driving frequencies.

The shapes and widths of the ion flux energy distribution functions at both electrodes also change as a function of the fundamental driving frequency, such as shown in figure 11 for $\gamma = 0.1$ and 0.4 at $\theta = 0^\circ$. At low frequencies, the distribution functions decay exponentially, while they show multiple peaks at lower energies caused by charge-exchange collisions inside the sheaths and a more pronounced high-energy tail at high frequencies. These differences are caused by the lower plasma density at lower frequencies. Thus, the sheath widths are bigger and the sheaths are more collisional at a given voltage at low compared with high frequencies. At high frequencies the distribution function extends to higher energies at the powered compared with the grounded electrode, while this situation is reversed at low frequencies. At high frequencies, the strongly negative dc self-bias, i.e. a higher mean sheath voltage at the powered electrode, causes the maximum ion energy to be higher at the powered side, while $\varepsilon \approx 1$, i.e. the maximum sheath voltages are identical at both electrodes. At low frequencies, however, the dc self-bias is strongly reduced, i.e. the mean sheath voltages are similar, but $\varepsilon > 1$, i.e. the maximum sheath voltage is higher at the grounded electrode. This causes the maximum ion energy to be higher at the grounded side at low frequencies. Experimental investigations of these effects are clearly required.

4. Conclusions

The effect of the fundamental driving frequency on the electrical asymmetry effect (EAE), i.e. the electrical generation of a dc self-bias, the control range of the mean ion energy, and the ion flux at both electrodes, has been investigated by PIC/MCC simulations and analytical modelling in dual-frequency capacitively coupled radio frequency discharges driven by two consecutive phase-locked harmonics with adjustable phase shift, θ. A strong decrease in the control range of the electrically induced dc self-bias and the mean ion energies at both electrodes as a function of θ was found at low compared with high fundamental driving frequencies. The control factor of the mean ion energy was found to be decreased from about 1.75 at 27.12 MHz to about 1.2 at 1 MHz. Although the ion flux to both electrodes remains fairly constant as a function of θ at all frequencies investigated, this result means that the EAE cannot be used effectively to control the mean ion energy at low driving frequencies in such discharges.

Based on the analytical model the decrease in the control range of the self-bias and the mean ion energy is found to be caused by an enhanced charge dynamics at low driving frequencies that affects the discharge symmetry and spatio-temporal ionization dynamics. Changing the electrode material, i.e. changing the secondary electron emission coefficient, γ, affects the electrical generation of a dc self-bias and the ion energy control primarily at high driving frequencies, where a higher γ leads to a stronger discharge asymmetry via the effect of secondary electrons on the ionization dynamics. This effect was found to work in a

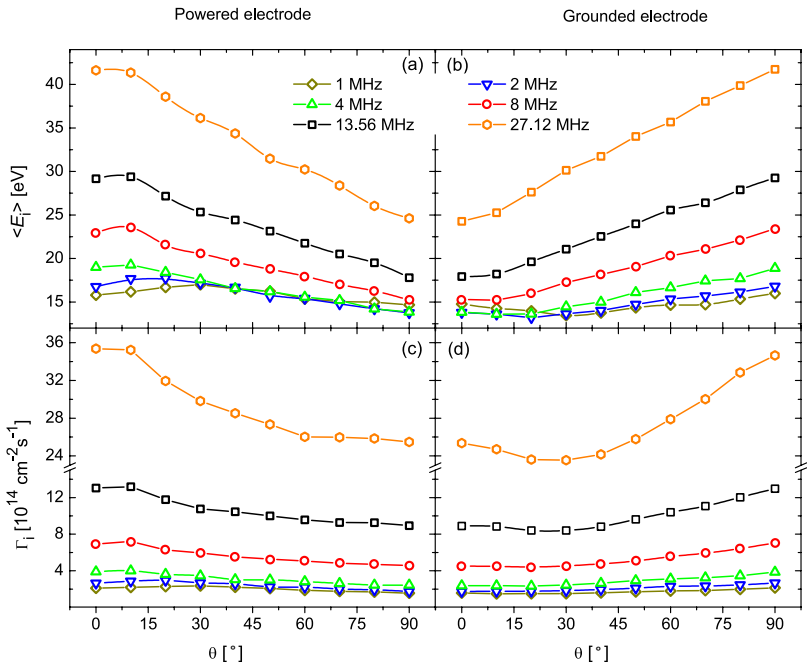

Figure 10. The ion mean energy $\langle E_i \rangle$ (top panels) and ion flux Γ_i (bottom panels) as a function of θ obtained for different frequencies from the PIC simulation for the powered (left panels) and grounded electrode (right panels).

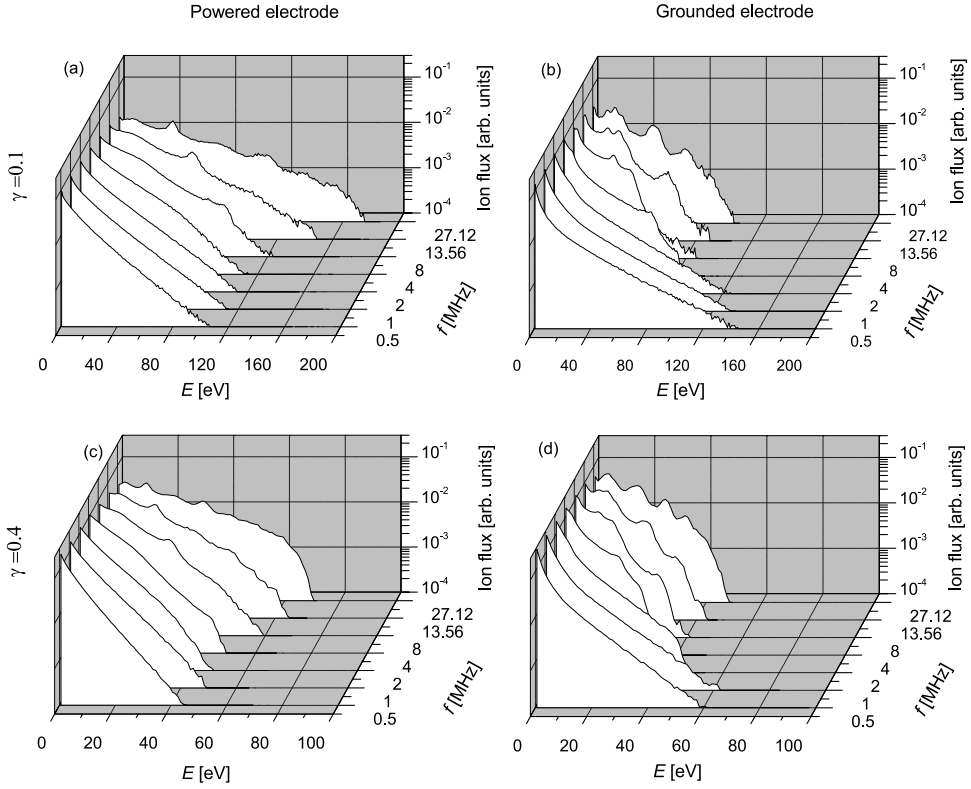

Figure 11. Ion flux energy distribution functions as a function of the fundamental driving frequency obtained from the PIC simulations at 50 Pa and $\theta = 0^\circ$: (*a*) $\gamma = 0.1$, powered electrode, (*b*) $\gamma = 0.1$, grounded electrode, (*c*) $\gamma = 0.4$, powered electrode, (*d*) $\gamma = 0.4$, grounded electrode.

completely different way at high and low driving frequencies. While at high frequencies a negative bias causes more ionization by secondary electrons at the powered electrode due to different time averaged sheath voltages, different maximum sheath voltages caused by the enhanced charge dynamics lead to more ionization by secondary electrons at the grounded electrode at low driving frequencies, although η remains negative.

For large area processing applications in CCPs, there is typically a high-frequency limit caused by radial inhomogeneities due to electromagnetic standing wave effects [19]. This work demonstrates that there will also be limitations

at low frequencies, if the EAE is used to realize the separate control of ion properties. Thus, a compromise must be found by choosing an intermediate frequency.

Acknowledgments

This work was supported by the Hungarian Scientific Research Fund (OTKA-K-77653, IN-85261 and K-105476).

References

[1] Makabe T and Petrović Z Lj 2006 *Plasma Electronics: Applications in Microelectronic Device Fabrication* (London: Taylor and Francis)
[2] Lieberman M A and Lichtenberg A J 2005 *Principles of Plasma Discharges and Materials Processing* 2nd edn (New York: Wiley Interscience)
[3] Georgieva V and Bogaerts A 2006 *Plasma Sources Sci. Technol.* **15** 368
[4] Lee S H, Tiwari P K and Lee J K 2009 *Plasma Sources Sci. Technol.* **18** 025024
[5] Mussenbrock T, Ziegler D and Brinkmann R P 2006 *Phys. Plasmas* **13** 083501
[6] Kawamura E, Lieberman M A and Lichtenberg A J 2006 *Phys. Plasmas* **13** 053506
[7] Boyle P C, Ellingboe A R and Turner M M 2004 *Plasma Sources Sci. Technol.* **13** 493
[8] Kitajima T, Takeo Y, Petrović Z Lj and Makabe T 2000 *Appl. Phys. Lett.* **77** 489
[9] Denda T, Miyoshi Y, Komukai Y, Goto T, Petrovic Z L and Makabe T 2004 *J. Appl. Phys.* **95** 870
[10] Wang S B and Wendt A E 2000 *J. Appl. Phys.* **88** 643
Patterson M M, Chu H-Y and Wendt A E 2007 *Plasma Sources Sci. Technol.* **16** 257
[11] Johnson E V, Delattre P A and Booth J P 2012 *Appl. Phys. Lett.* **100** 133504
[12] Johnson E V, Verbeke T, Vanel J-C and Booth J P 2010 *J. Phys. D: Appl. Phys.* **43** 412001
[13] Novikova *et al* 2012 *39th European Physical Society Conf. on Plasma Physics and 16th Int. Congress on Plasma Physics (Stockholm, Sweden, 2–6 July 2012)*
Lafleur T and Booth J P 2012 *J. Phys. D: Appl. Phys.* **45** 395203
Lafleur T *et al* 2012 *Appl. Phys. Lett.* **101** 124104
[14] Baloniak T, Reuter R and von Keudell A 2010 *J. Phys. D: Appl. Phys.* **43** 335201
[15] Rauf S and Kushner M J 1999 *IEEE Trans. Plasma Sci.* **27** 1329
[16] Kawamura E, Lieberman M A, Lichtenberg A J and Hudson E A 2007 *J. Vac. Sci. Technol.* A **25** 1456
Kawamura E, Lichtenberg A J and Lieberman M A 2008 *Plasma Sources Sci. Technol.* **17** 045002
[17] Jiang W, Xu X, Dai Z L and Wang Y N 2008 *Phys. Plasmas* **15** 033502
[18] Schulze J, Schuengel E and Czarnetzki U 2012 *Appl. Phys. Lett.* **100** 024102
[19] Lieberman M A, Booth J P, Chabert P, Rax J M and Turner M M 2002 *Plasma Source Sci. Technol.* **11** 283
[20] Chabert P, Raimbault J L, Rax J M and Perret A 2004 *Phys. Plasmas* **11** 4081
[21] Yang Y and Kushner M J 2010 *J. Phys. D: Appl. Phys.* **43** 152001
[22] Schulze J, Gans T, O'Connell D, Czarnetzki U, Ellingboe A R and Turner M M 2007 *J. Phys. D: Appl. Phys.* **40** 7008
[23] Gans T, Schulze J, O'Connell D, Czarnetzki U, Faulkner R, Ellingboe A R and Turner M M 2006 *Appl. Phys. Lett.* **89** 261502
[24] Turner M M and Chabert P 2006 *Phys. Rev. Lett.* **96** 205001
[25] Waskoenig J and Gans T 2010 *Appl. Phys. Lett.* **96** 181501
[26] Donkó Z 2007 *Proc. Symp. Application of Plasma Processes (Podbanske, Slovakia 20–25 January 2007)* ed J Matuska *et al* pp 21–4, IL02
[27] Booth J P, Curley G, Marić D and Chabert P 2010 *Plasma Sources Sci. Technol.* **19** 015005
[28] Schulze J, Donkó Z, Schüngel E and Czarnetzki U 2011 *Plasma Sources Sci. Technol.* **20** 045007
Donkó Z, Schulze J, Hartmann P, Korolov I, Czarnetzki U and Schüngel E 2010 *Appl. Phys. Lett.* **97** 081501
[29] Heil B G, Schulze J, Mussenbrock T, Brinkmann R P and Czarnetzki U 2008 *IEEE Trans. Plasma Sci.* **36** 1404
Heil B G, Czarnetzki U, Brinkmann R P and Mussenbrock T 2008 *J. Phys. D: Appl. Phys.* **41** 165202
[30] Schulze J, Schüngel E and Czarnetzki U 2009 *J. Phys. D: Appl. Phys.* **42** 092005
[31] Donkó Z, Schulze J, Heil B G and Czarnetzki U 2009 *J. Phys. D: Appl. Phys.* **42** 025205
[32] Bora B, Bhuyan H, Favre M, Wyndham E and Chuaqui H 2012 *Appl. Phys. Lett.* **100** 094103
[33] Zhang Q-Z, Zhao S-X, Jiang W and Wang Y-N 2012 *J. Phys. D: Appl. Phys.* **45** 305203
[34] Longo S and Diomede P 2009 *Plasma Process. Polym.* **6** 370
[35] Schüngel E, Zhang Q-Z, Iwashita S, Schulze J, Hou L-J, Wang Y-N and Czarnetzki U 2011 *J. Phys. D: Appl. Phys.* **44** 285205
[36] Schulze J, Derzsi A and Donkó Z 2011 *Plasma Sources Sci. Technol.* **20** 024001
[37] Schulze J, Schüngel E, Czarnetzki U and Donkó Z 2009 *J. Appl. Phys.* **106** 063307
[38] Schulze J, Schüngel E, Donkó Z and Czarnetzki U 2011 *Plasma Sources Sci. Technol.* **20** 015017
[39] Olevanov M, Proshina O, Rakhimova T and Voloshin D 2008 *Phys. Rev.* E **78** 026404
[40] Braginsky O, Kovalev A, Lopaev D, Proshina O, Rakhimova T, Vasilieva A, Voloshin D and Zyryanov S 2012 *J. Phys. D: Appl. Phys.* **45** 015201
[41] Proshina O, Rakhimova T V and Rakhimov A T 2006 *Plasma Sources Sci. Technol.* **15** 402
[42] Georgieva V and Bogaerts A 2005 *J. Appl. Phys.* **98** 023308
[43] Georgieva V, Bogaerts A and Gijbels R 2004 *Phys. Rev.* E **69** 026406
[44] Birdsall C K 1991 *IEEE Trans. Plasma Science* **19** 65
[45] Verboncoeur J P 2005 *Plasma Phys. Control. Fusion* **47** A231
[46] Matyash K, Schneider R, Taccogna F, Hatayama A, Longo S, Capitelli M, Tskhakaya D and Bronold F X 2007 *Contrib. Plasma Phys.* **47** 595
[47] Phelps A V and Petrović Z Lj 1999 *Plasma Sources Sci. Technol.* **8** R21
Phelps A V 1994 *J. Appl. Phys.* **76** 747
Phelps A V http://jilawww.colorado.edu/~avp/collision_data/ unpublished
[48] Kollath R 1956 *Encyclopedia of Physics* vol XXI ed S Flügge (Berlin: Springer) p 264
[49] Hrunski D *et al* 2013 *Vacuum* **87** 114
[50] Schulze J, Derzsi A, Dittmann K, Hemke T, Meichsner J and Donkó Z 2011 *Phys. Rev. Lett.* **107** 275001
Liu Y-X *et al* 2012 *Appl. Phys. Lett.* **101** 114101
[51] Czarnetzki U, Schulze J, Schüngel E and Donkó Z 2011 *Plasma Sources Sci. Technol.* **20** 024010
[52] Schulze J, Schüngel E, Donkó Z and Czarnetzki U 2010 *J. Phys. D: Appl. Phys.* **43** 225201
[53] Belenguer Ph and Boeuf J-P 1990 *Phys. Rev.* A **41** 4447